Journal of Colloid and Interface Science 505 (2017) 796–804

Contents lists available at ScienceDirect

Journal of Colloid and Interface Science

journal homepage: www.elsevier.com/locate/jcis

Regular Article

Facile synthesis of ultrafine cobalt oxide nanoparticles for high-performance supercapacitors

Fangyan Liu, Hai Su, Long Jin, Haitao Zhang, Xiang Chu, Weiqing Yang *

State Key Laboratory of Traction Power, School of Materials Science and Engineering, Southwest Jiaotong University, Chengdu 610031, China

GRAPHICAL ABSTRACT

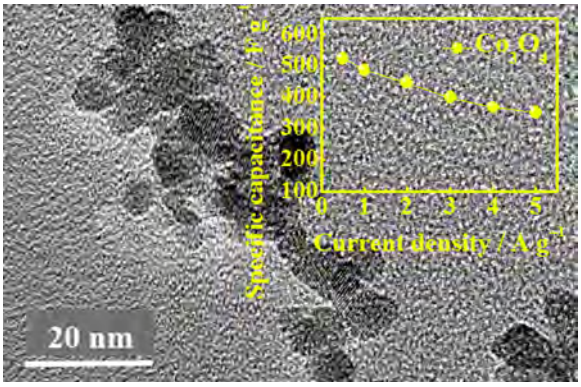

ARTICLE INFO

Article history:
Received 1 May 2017
Revised 14 June 2017
Accepted 19 June 2017
Available online 20 June 2017

Keywords:
Cobalt oxide
Ultrafine nanoparticles
Supercapacitor
Electrochemical performance

ABSTRACT

The ultrafine Co_3O_4 nanoparticles are successfully prepared by a novel solvothermal–precipitation approach which exploits the supernatant liquid of Co_3O_4 nanoflake micropheres synthesized by solvothermal method before. Interestingly, the water is only employed to obtain the ultrafine nanoparticles in supernatant liquid which was usually thrown away before. The microstructure measurement results of the as-grown samples present the homogeneous disperse ultrafine Co_3O_4 nanoparticles with the size of around 5–10 nm. The corresponding synthesis mechanism of the ultrafine Co_3O_4 nanoparticles is proposed. More importantly, these ultrafine Co_3O_4 nanoparticles obtained at 250 °C show the highest specific capacitance of 523.0 F g^{-1} at 0.5 A g^{-1}, 2.6 times that of Co_3O_4 nanoflake micropheres due to the quantum size effect. Meanwhile, the sample annealed under 350 °C possesses the best cycling stability with capacitance retention of 104.9% after 1500 cycles. These results unambiguously demonstrate that this work not only provides a novel, facile, and eco-friendly approach to prepare high-performance Co_3O_4 nanoparticles electrode materials for supercapacitors but also develops a widely used method for the preparation of other materials on a large scale.

1. Introduction

With the fast development of the world economy, the growing consumption of fossil fuels, and increasing aggravation of environmental pollution, the insistent demand for highly efficient, stable, environmentally friendly, and sustainable sources of energy has

* Corresponding author at: Key Laboratory of Advanced Technologies of Materials (Ministry of Education), School of Materials Science and Engineering, Southwest Jiaotong University, No. 111, North 1st Section of Second Ring Road, Jinniu District, Chengdu 610031, China.
E-mail address: wqyang@swjtu.edu.cn (W. Yang).

http://dx.doi.org/10.1016/j.jcis.2017.06.058
0021-9797/

prompted considerable research efforts for energy storage/conversion technologies [1–3]. In recent years, electrochemical capacitors (ECs) have attracted considerable research interest as an important energy storage device, mainly due to their higher energy density than conventional capacitors and higher power density than batteries as well as high energy density, fast charge and discharge capability, and excellent cycling performance [4,5]. Generally, according to the energy storage mechanisms, the supercapacitor can be generally categorized as electrical double-layer capacitors (EDLCs) and electrochemical pseudocapacitors (EPCs) [6,7]. Because of the large specific capacitance and fast redox kinetics of EPCs [8,9], the research on the electrochemical pseudocapacitors has attracted enormous attention so far. The electroactive materials in electrodes are the pivotal factor which can greatly influence the electrochemical properties of pseudocapacitors [10,11], hence, looking for high performance electrode materials is a key issue for the supercapacitor development [11].

Metal oxides and hydroxides have occupied a very important position in electroactive materials. Among them, cobalt oxide (Co_3O_4), as an important transition metal oxide, has attracted special attention and been widely studied as a pseudocapacitive material for supercapacitor applications, attributed to its potential as a promising replacement for the RuO_2 because of its high theoretical capacity (3560 F g^{-1}), low cost, practical availability, and eco-friendly nature [12,13]. In the last decade, the significant progress in the synthesis of nanoscaled Co_3O_4 with controlled size, structure, and morphology has been achieved, which is expected to acquire the desirable materials with high capacitive performance. Up to now, Co_3O_4 with various morphologies and nanostructures, including nanowire [14], nanosheet [15], nanoflower [16], nanoparticles [12], nanorods [17], urchin-like [18], and hollow structure [9,10] etc., have been prepared successfully and used as the building blocks to design and fabricate the high-performance supercapacitors.

It has been established that nanoscaled active materials with small particle size and high surface/volume ratio which could decrease mass and charge diffusion distances and provide more active sites can make the most of active materials and then improve their electrochemical performances in contrast to their bulk counterparts [7,13,19]. For instance, Vijayakumar et al. adopted microwave assisted method to synthesize 24 nm Co_3O_4 nanoparticles with the maximum specific capacitance of 519 F g^{-1} at 0.5 mA cm^{-2} [20]. Tummala et al. used the plasma spray technique directly depositing the 10–50 nm Co_3O_4 nanoparticles on the current collectors [19]. However, the special experimental apparatuses mentioned in above reports greatly limit the widespread use of the synthetic methods to acquire Co_3O_4 nanoparticles on a large scale. In order to overcome these disadvantages, numerous studies have been carried out to seek for simple and efficient approaches to acquire high performance Co_3O_4 nanoparticles. For example, Deng et al. synthesized Co_3O_4 and Co_3O_4/CoO nanoparticles through a one-step solution combustion process, which presented a capacitance of 362.8 F g^{-1} at 0.2 A g^{-1} after annealing [12]. Li et al. obtained the Co_3O_4 nanoparticles via a low temperature solution process at 70 °C and utilized for pseudosupercapacitors with a reasonable specific capacitance of 304 F g^{-1} at 5 mV s^{-1} [21]. Obviously, the simple experimental apparatuses and methods in above reports are followed by unsatisfactory electrochemical performances. Meanwhile, the overall sizes of nanomaterials in above reports were usually decades of nanometers or even hundreds of nanometers, which would limit the specific surface area of the as-grown samples and then restrict their specific capacitance. Consequently, it is still a big challenge to prepare ultrafine Co_3O_4 nanoparticles with excellent electrochemical properties on a large scale via a facile way.

In this study, we developed a novel, facile, and eco-friendly sol vothermal–precipitation approach for synthesizing ultrafine Co_3O_4 nanoparticles. Interestingly, the ultrafine nanoscaled precursor was easily synthesized by adding water into the supernatant liquid left after centrifugation. The precursor and Co_3O_4 nanoparticles were characterized in terms of their physical and chemical properties such as phase structure, morphological properties, and chemical composition. Furthermore, a possible synthesis mechanism of the Co_3O_4 nanoparticles was discussed in detail. Finally, the capacitive performances of the Co_3O_4 nanoparticles obtained under different annealing temperatures were investigated. Particularly, the Co_3O_4 nanoparticles annealed at 250 °C possessed the highest specific capacitance of 523.0 F g^{-1} at 0.5 A g^{-1}, while the sample obtained at 350 °C exhibited the best cycling stability with capacitance retention of 104.9% after 1500 cycles. To the best of our knowledge, this is the first study to synthesize the ultrafine Co_3O_4 nanoparticles precursor just by adding water into the supernatant liquid left after centrifugation.

2. Experimental

2.1. Synthesis of ultrafine Co_3O_4 nanoparticles samples

All chemicals were of analytical grade and used as received without further purification. Cobalt acetate tetrahydrate ($Co(CH_3COO)_2{\cdot}4H_2O$, 99.5%) was purchased from Aladdin Industrial Corporation. Urea ($CO(NH_2)_2$, 99.0%) and ethanol (C_2H_5OH, 99.7%) were purchased from Chengdu Kelon Chemical Reagent Factory.

The main preparation process of the Co_3O_4 nanoparticles precursor is shown schematically in Fig. 1. In this typical synthesis procedure, 0.623 g cobalt acetate tetrahydrate ($Co(CH_3COO)_2{\cdot}4H_2O$) and 1.4 g urea ($CO(NH_2)_2$) were dissolved in 20 mL ethanol by ultrasonic dispersion. Then, the obtained mixture was transferred into a 40 mL Teflon-lined autoclave and then sealed, which was then heated in an oven at 160 °C for 2 h and then cooled to ambient temperature. The solid products which are the Co_3O_4 nanoflake microspheres were collected by a centrifugation–redispersion process, washed with ethanol for several times and used for pseudocapacitors by our group before [22].

The rest supernatant liquid which was usually thrown away before was used to prepare the ultrafine Co_3O_4 nanoparticles by adding enough ultrapure water into it (V_{water}:$V_{supernatant\ liquid}$ = 1:10), then let stand for 72 h in ambient temperature. It can be seen that there were some precipitates coming into being gradually. The Co_3O_4 precursor was collected by centrifugation and washed with water for several times. Then the final product was dried in an oven at 70 °C for one night. For the synthesis of Co_3O_4 nanostructures, the as-prepared precursor was heated to 200, 250, 300, and 350 °C with a heating rate of 1 °C min^{-1} and kept for 10 min in air, respectively. In brief, the products obtained under different conditions were named sample-I, sample-II, sample-III, and sample-IV, respectively.

2.2. Characterizations

Thermogravimetric analysis of the precursor was investigated using a Q50 thermogravimetric analyzer with a heating rate of 10 °C min^{-1} from ambient temperature to 700 °C in air. The crystal structure properties of the products were determined by using the XPert Pro MPD (Holland) X-ray diffractmeter with Cu K_{a1} radiation (λ = 0.154 nm). The Fourier transform infrared (FTIR) instrument (Magna 560, Nicolet, Thermo Electron Corp., USA) was used to record the Fourier-Transform Infrared (FTIR) spectra. The samples were investigated in the wavenumber range of 400–4000 cm^{-1} using 32 scans with a spectral resolution of 4 cm^{-1}. The morphol-

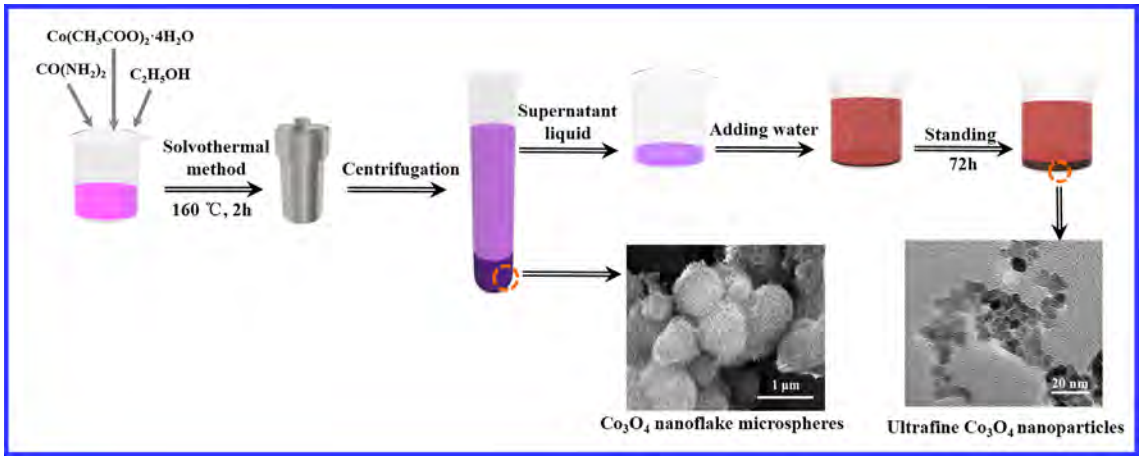

Fig. 1. Synthesis procedure for ultrafine Co_3O_4 nanoparticles precursor. (The SEM image of Co_3O_4 nanoflake microspheres has been published by our group [22].)

ogy and structure of the samples were characterized by field-emission scanning electron microscopy (FESEM) (JEOL, JSM-7001F). Transmission electron microscopy (TEM) and high-resolution TEM (HRTEM) were carried out on a JEOL JSM- 2100F operating at an accelerating voltage of 200 kV. The Micromeritics ASAP 2020 surface area and pore size analyzer was applied to investigate the Brunauer-Emmertt-Teller (BET) surface areas and Barrett-Joyner-Halenda (BJH) pore size distribution of the samples using N_2 adsorption-desorption isotherms recorded at 77 K.

2.3. Electrochemical measurements

The electrochemical performances were carried out on a CHI660E electrochemical working station (Shanghai Chenhua Instrument, Inc.). The three-electrode system was adopted in 6.0 M KOH aqueous electrolyte. The Pt plate electrode was used as the counter electrode, while the Hg/HgO electrode as the reference electrode. The working electrode was prepared by mixing the active material, polytetrafluoroethylene binder, and acetylene black at a weight ratio of 8:1:1 in ethanol. The mixture was mixed under ultrasonic vibration for about 1 h, and dried in air at 85 °C for 8 h to remove the excess ethanol. After this, the mixture was rolled into 100–120 μm thick film after being kneaded thoroughly. After drying at 105 °C for 12 h, a part of the thin film (1.13 cm^2) was taken out and pressed onto the nickel foam, and the electrode plate was further compacted mechanically.

The electrochemical performances of the samples were studied with cyclic voltammetry (CV) and galvanostatic charge-discharge (GCD) tests. The cycle-life tests of the samples were measured on Land Series Batteries Testing System (Wuhan Land Electronic Co., LTD). The specific capacitances of active materials can be calculated according to the following equation:

$$C = I\Delta t/(m\Delta V) \quad (1)$$

where C ($F\,g^{-1}$) is the specific capacitance, I (A) represents the discharge current, Δt (s) is the discharging time, m (g) represents the mass of active material, and ΔV (V) is the potential window.

3. Results and discussion

3.1. Structural and morphological properties of the Co_3O_4 precursor and Co_3O_4 nanoparticles obtained after annealing treatment

The thermal stability of the precursor was investigated through the way of TGA analysis, presented in Fig. S1. About 6.5% weight loss is found below 128 °C, which is caused by the removal of the physically adsorbed water. From 128 to 350 °C, the precursor is thermally unstable and continuous decomposition. In order to obtain the optimal temperature for the production of Co_3O_4 nanoparticles, the annealing temperature is selected from 200 to 350 °C. The XRD patterns of the as-prepared precursor and annealed Co_3O_4 nanoparticles samples are displayed in Figs. S2 and 2, respectively. It is clearly observed that there is no obvious diffraction peak for the as-prepared precursor (Fig. S2), suggesting that the precursor is an amorphous chemical compound of cobalt, while the annealed products after heat-treatment at 200, 250, 300, and 350 °C belong to the cubic spinel Co_3O_4 phase (JCPDS Card no. 43-1003). The Co_3O_4 nanoparticles samples I–IV exhibit typical diffraction peaks at 19.2, 31.4, 36.8, 44.9, 55.7, 59.3, and 65.3°, which correspond to (111), (220), (311), (400), (422), (511), and (440) crystal planes of the cubic spinel Co_3O_4 phase, respectively, indicating the formation of the crystalline Co_3O_4 nanoparticles. Because of the increment of annealing temperature, the corresponding products exhibit higher diffraction intensities and stronger crystallization properties. Furthermore, the crystal size of different Co_3O_4 nanoparticles increases gradually from 5.5 to 10.5 nm when the temperature increases from 200 to 350 °C (crystal sizes estimated according to the Scherer formula: 5.5, 7.5, 8.6, and 10.5 for sample-I, -II, -III, and -IV, respectively).

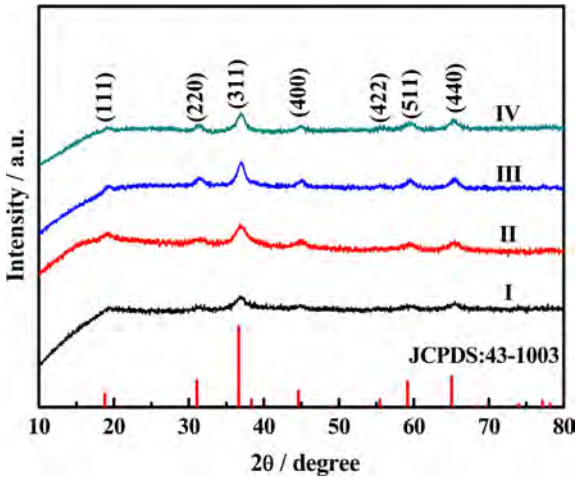

Fig. 2. XRD spectra of the Co_3O_4 samples I–IV acquired at different annealing temperatures. The bar at the bottom in figure indicates the standard lines of Co_3O_4 (JCPDS Card no. 43-1003).

The FESEM images are applied to investigate the microstructures and morphologies of the precursor and Co_3O_4 samples I–IV in Fig. 3. Notice that in Fig. 3a, the as-synthetized precursor is uniformly formed of countless nanoparticles which are approximately 15–25 nm in size, presenting an irregular shape with rough surface. The homogenous shape and size of the Co_3O_4 precursor is attributable to the slow precipitation during the forming process. Fig. 3b and c depict the morphologies of the sample-I and sample-II obtained at 200 and 250 °C, in which the samples I-II were found uniformly distributed, but still with partially mild granular agglomeration. These nanoparticles possess rough surface and arrange randomly, which facilitates the formation of pore structure and then provides short transport pathways for electrolyte ions, and thus helps the Faradic reaction [23]. However, compared with the Co_3O_4 samples I–II, the agglomerate state of the samples III–IV becomes more and more serious with annealing temperature elevating (Fig. 3d and e). It can be observed that the sample III is mainly composed of the numerous agglomerated tiny particles, while the sample IV is found consisting of large pieces, which can lead to the disappearance of the pore structure and the decrease of specific surface area.

To further characterize the Co_3O_4 nanoparticles, the sample-II is selected and evaluated by TEM (Fig. 4). As shown in Fig. 4a and b, the Co_3O_4 nanoparticles are uniformly distributed and the size of them is around 5–10 nm which is much smaller than that of the precursor. Furthermore, the measured lattice spacings of 0.245, 0.288, and 0.462 nm are in good agreement with the (311), (220), and (111) interplanar distances of cubic phase of Co_3O_4 (Fig. 4c), which coincides with the results of XRD. Similar result is obtained from the SAED pattern in Fig. 4d. The HRTEM and the diffraction rings in the SAED pattern indicate that the ultrafine Co_3O_4 nanoparticles are polycrystalline in nature.

Additionally, the nitrogen adsorption-desorption isotherms were collected for Co_3O_4 samples I–IV to determine their BET specific surface area and BJH pore size distribution, which is highly relevant to their electrochemical performances (Fig. 5). According to the IUPAC classification, all samples display the type IV isotherms, indicating the existence of mesopores in these samples [24]. According to the experimental results, the specific surface area, pore size distribution, and pore volume of Co_3O_4 samples are dramatically different. The BET specific surface areas and the BJH desorption pore volumes were 188.4, 196.9, 164.0, 91.6 $m^2 g^{-1}$ and 0.166, 0.195, 0.488, 0.262 $cm^3 g^{-1}$ for sample-I, -II, -III, and -IV, respectively. As shown in Fig. 5b, the pores size in sample-I mainly locates at 1.8 nm and 4.3 nm, indicating that the pores in sample-I mostly consist of micropores and mesopores. The sample-II displays a narrow pore-size distribution at around 2 nm. Whereas, sample-III exhibits a mesoporous structure with a sharp peak at 2.5 nm as well as a macroporous structure with a wide pore-size distribution at 90 nm. For sample-IV, the pore size distribution is in a relatively wide range and focused on around 12 nm, showing the mesoporous structure. According to the results of SEM and TEM, it can be inferred that the micropores and mesopores in these Co_3O_4 samples mainly are the space among the nanoparticles. As for the macroporous in the samples III–IV, they almost come from the space stacked by the large agglomerated particles. The mesoporous structure in samples with higher pore volume can facilitate the diffusion and transport of electrolyte ions in the charge/discharge process, and the larger specific surface area is of huge benefits for the increase of the electrolyte/electrode contact area, then provide more active sites for Faraday reaction, which is helpful to achieve excellent electrochemical performance.

3.2. The possible synthesis mechanism of Co_3O_4 precursor

To further study the precursor and the Co_3O_4 sample obtained after annealing at 250 °C, FTIR analysis was carried out (Fig. 6). As presented in the FTIR spectrum of the Co_3O_4 sample-II, the strong peak centered at 3400 and the peak at 1625 cm^{-1} correspond to the surface absorbed water and surface hydroxyls in nanocrystals' surface [25]. The sharp peaks at 663 and 569 cm^{-1} are attributed to the stretching vibration of Co^{2+}—O bond and Co^{3+}—O bond of the spinel cobalt oxide [26,27], respectively, giving obvious evidence for the existence of the crystalline Co_3O_4. As presented in the black curve in Fig. 3b, the broad band at 3428 cm^{-1} is assigned to the hydrogen-bond O—H groups and stretching vibra-

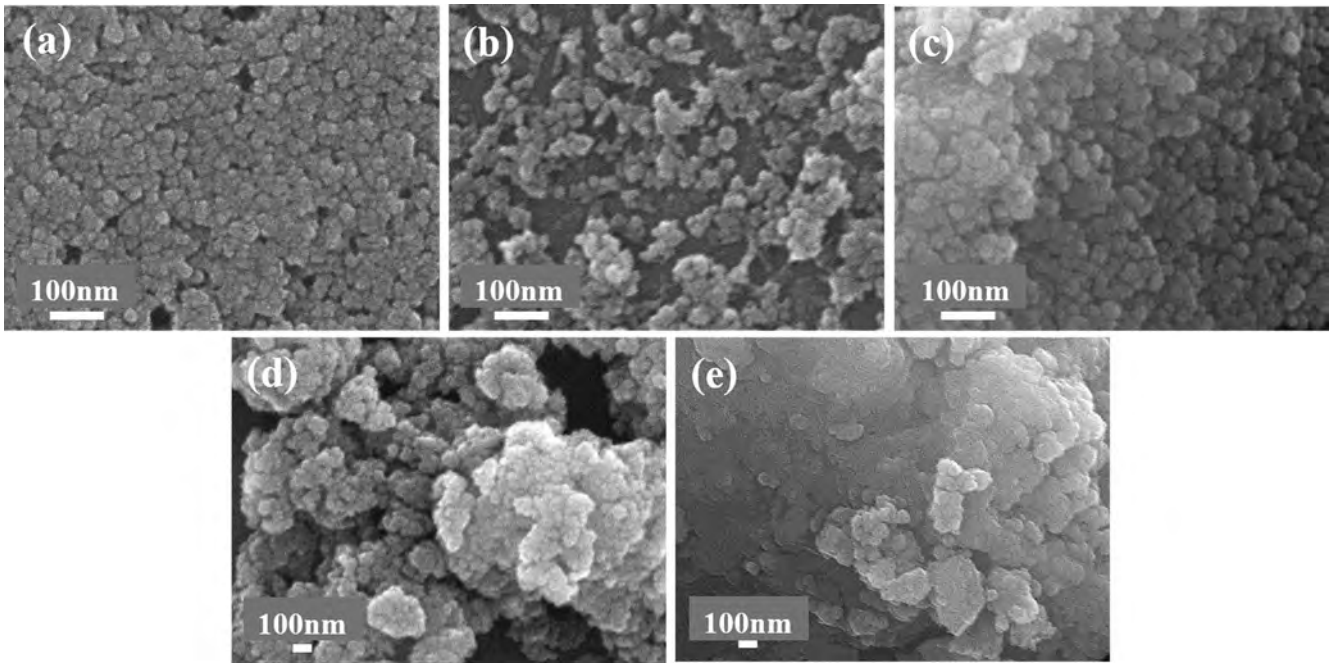

Fig. 3. Different magnification SEM images of (a) precursor and Co_3O_4 nanoparticles obtained at (b) 200, (c) 250, (d) 300, and (e) 350 °C.

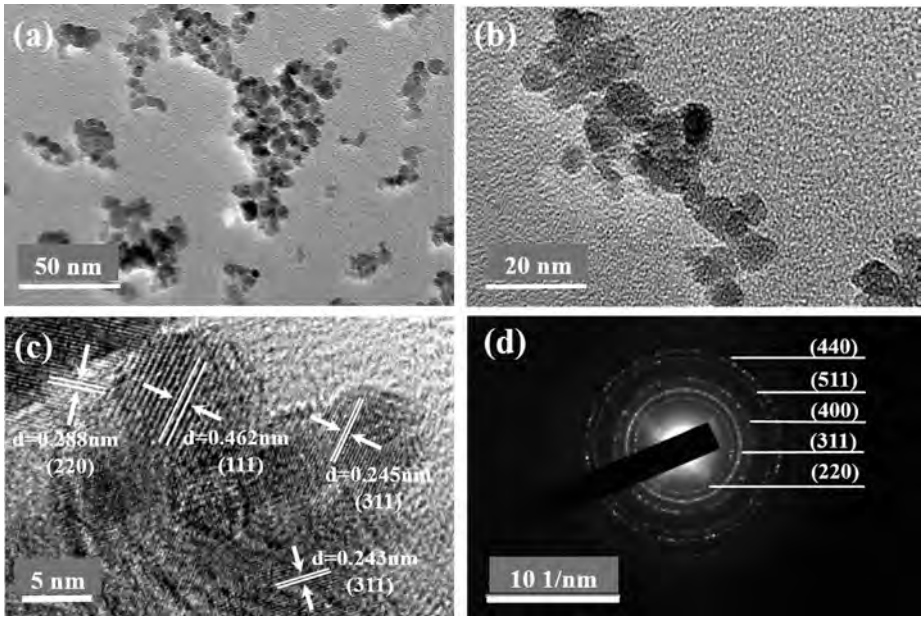

Fig. 4. (a and b) TEM images, (c) HRTEM image, and (d) SAED pattern of ultrafine Co_3O_4 nanoparticles obtained after heat treatment at 250 °C.

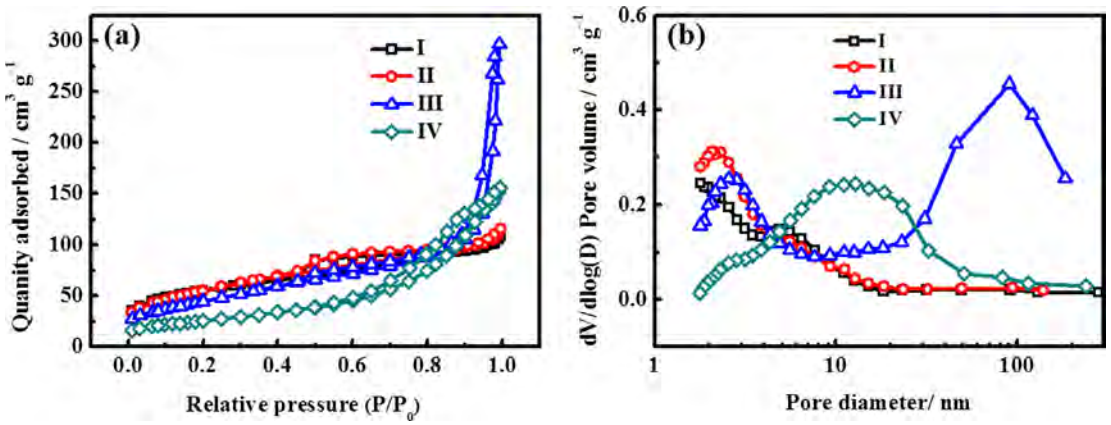

Fig. 5. (a) Nitrogen adsorption–desorption isotherms and (b) pore size distributions of Co_3O_4 samples I–IV.

tion of O—H in molecular water [9]. The peaks observed at 1465, 1348, 830, 1057, 739, and 659 cm^{-1} are assigned to $\nu(CO_3)$, C—O, $\delta(CO_3)$, ν(C═O), δ(OCO), and ρ(OCO), respectively [28–31], which evidence the presence of CO_3^{2-} in the precursor. Hence, the as-synthesized precursor could be defined as the cobalt carbonate compound. A possible synthesis mechanism of the precursor is discussed as follows. In the solvothermal reaction, the urea is first thermally decomposed into ammonia (NH_3) and isocyanic acid (HNCO) according to Eq. (2) [32,33]. HNCO formed in reaction (2) then reacts with water and produces ammonia (NH_3) and carbon dioxide (CO_2) according to Eq. (3) [32], then NH_3 and CO_2 hydrolyze to produce the OH^- and CO_3^{2-} via Eqs. (4) and (5) [34,35]. Due to the limited water which mainly comes from the crystal water in cobalt acetate tetrahydrate, the NH_3 and CO_2 produced in these reactions do not hydrolyze into OH^- and CO_3^{2-} completely, and part of them still exist in the liquid.

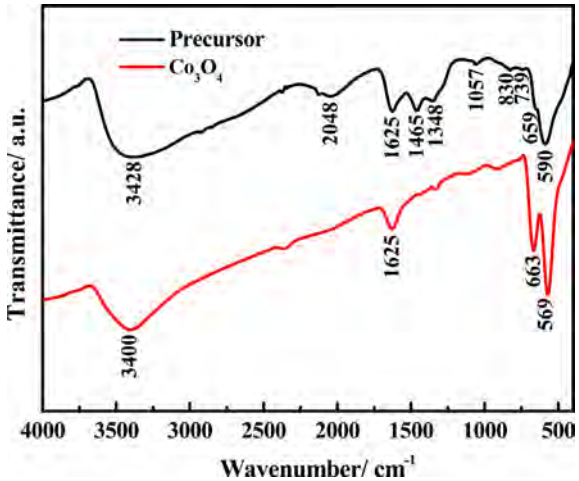

Fig. 6. FTIR curves of the Co_3O_4 precursor and the sample-II obtained at 250 °C.

$$H_2NCONH_2 \rightarrow NH_4^+NCO^- \rightarrow NH_3 + HNCO \quad (2)$$

$$HNCO + H_2O \rightarrow NH_3 + CO_2 \quad (3)$$

$$NH_3 + H_2O \rightarrow NH_4^+ + OH^- \quad (4)$$

$$CO_2 + H_2O \rightarrow CO_3^{2-} + 2H^+ \quad (5)$$

The aqueous ammonia solution has been recognized as a chemical absorbent for CO_2 capture [36,37], after adding water into the supernatant liquid obtained after centrifugation, the reactions happened in the solution are known to be very complicated. In order to easy to understand, the reversible reactions happened can be simplified as the following formulas [36,37]:

$$2NH_3 + CO_2 + H_2O \leftrightarrow (NH_4)_2CO_3 \quad (6)$$

$$NH_3 + CO_2 + H_2O \leftrightarrow NH_4HCO_3 \leftrightarrow NH_4^+ + HCO_3^- \quad (7)$$

$$NH_3 + H_2O \leftrightarrow NH_4^+ + OH^- \quad (8)$$

$$CO_2 + H_2O \leftrightarrow HCO_3^- + H^+ \quad (9)$$

$$HCO_3^- \leftrightarrow CO_3^{2-} + H^+ \quad (10)$$

Along with the above reactions going on, the CO_3^{2-} slowly deposits metal ion Co^{2+} which didn't participate in the solvothermal reaction to form $CoCO_3$ according to Eq. (11), which makes the CO_3^{2-} produced continually, and then more $CoCO_3$ forms. The precipitator CO_3^{2-} forms slowly in the solution so it can be found that there are no much precipitate coming into being in the early reaction period. In the annealing process, the precursor reacts with O_2 in air to convert into Co_3O_4 according to Eq. (12). However, the further research is still needed to investigate the more detailed formation mechanism of the Co_3O_4 nanoparticles.

$$Co^{2+} + CO_3^{2-} \rightarrow CoCO_3 \quad (11)$$

$$6CoCO_3 + O_2 \rightarrow 2Co_3O_4 + 6CO_2 \quad (12)$$

3.3. The electrochemical performances of Co_3O_4 nanoparticles

A series of electrochemical measurements are made to evaluate the properties of the ultrafine Co_3O_4 nanoparticles by applying them as the electroactive materials for pseudocapacitor electrodes. In order to compare the electrochemical performances of the Co_3O_4 nanoparticles obtained at different temperatures, the cyclic voltammetry (CV) and galvanostatic charge-discharge (GCD) tests are performed.

Fig. 7a exhibits the cyclic voltammetry curves of Co_3O_4 samples I–IV at the scan rate of 5 mV s^{-1} in the potential range of 0–0.6 V. Different from an ideal rectangular shape of the electric double-layer capacitance, the CV curves of all Co_3O_4 samples present two typical redox couples which are from the redox processes of Co_3O_4/CoOOH/CoO_2, indicating the faradic redox reaction nature of these materials in the electrochemical process. The first redox couple A_1/C_1 can be attributed to the reversible reaction between Co_3O_4 and CoOOH, expressed as Eq. (13) [38–40]:

$$Co_3O_4 + H_2O + OH^- \leftrightarrow 3CoOOH + e^- \quad (13)$$

While, the second redox couple A_2/C_2 corresponds to the conversion between CoOOH and CoO_2, described as Eq. (14) [38–40]:

$$CoOOH + OH^- \leftrightarrow CoO_2 + H_2O + e^- \quad (14)$$

Comparing the areas of the CV curves of Co_3O_4 samples, the area of sample-II is apparently much larger than those of other samples, indicating a higher specific capacitance of sample-II. The areas of CV curves of Co_3O_4 samples under different annealing temperatures are different, suggesting that controlling the annealing temperature can effectively control the electrochemical performance of Co_3O_4 nanoparticles. Fig. 7b presents the GCD curves of samples I–IV at current density of 0.5 A g^{-1} in the potential window of 0–0.5 V. It is well observed that there are two plateaus on the discharge curves, corresponding to the two sequential redox reactions as expressed by Eqs. (13) and (14). The shapes of all the galvanostatic charge-discharge curves with two potential decay stages on the discharge curves further present typical pseudocapacitive behavior of the samples, which is consistent well with the analysis of CV tests. According to the GCD curves, the specific capacitances of sample-I, -II, -III, and -IV are calculated to be 435.5, 523.0, 389.1, and 349.0 F g^{-1} at 0.5 A g^{-1}, respectively. Obviously, the specific capacitance of the ultrafine Co_3O_4 nanoparticles first increases with temperature elevating from 200 to 250 °C, then decreases when temperature increases from 250 to 350 °C. Both measurements indicate that the ultrafine Co_3O_4 nanoparticles obtained at 250 °C possess the best specific capacitance among these samples. This is due to that the sample-II has the larger specific surface area than that of others, which can increase the contact area between active materials and electrolyte and contribute to the specific capacitance; even though the pore volume of sample-II is smaller than that of samples III–IV, the order degree of crystals in samples III–IV obtained in the recrystallization process is higher due to the higher crystallinity, leading to the decrease of active sites, which goes against the specific capacitance.

The CV curves of sample-II at the various scan rates ranging from 2–50 mV s^{-1} within the potential window of 0–0.6 V are shown in Fig. 8a. The nonrectangular shapes of the CV curves reveal that the charge storage is a pseudocapacitance process coming from the conversion between different cobalt oxidation states and the corresponding faradaic reactions [22]. Along with the increment of scan rate, the anodic and cathodic peaks shift to higher and lower potentials, respectively, possibly due to polariza-

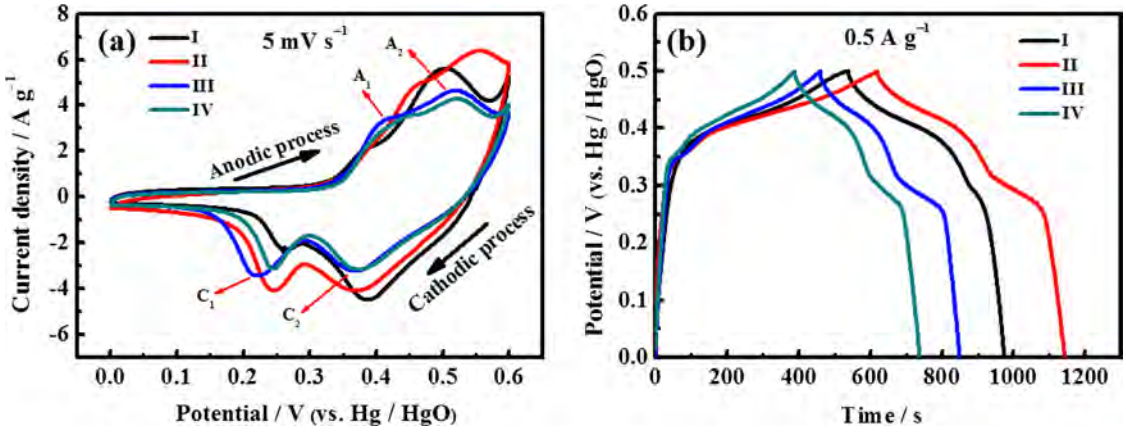

Fig. 7. (a) CV curves of Co_3O_4 samples I–IV at the scan rate of 5 mV s^{-1}. (b) Galvanostatic charge–discharge curves of Co_3O_4 samples I–IV at the current density of 0.5 A g^{-1}.

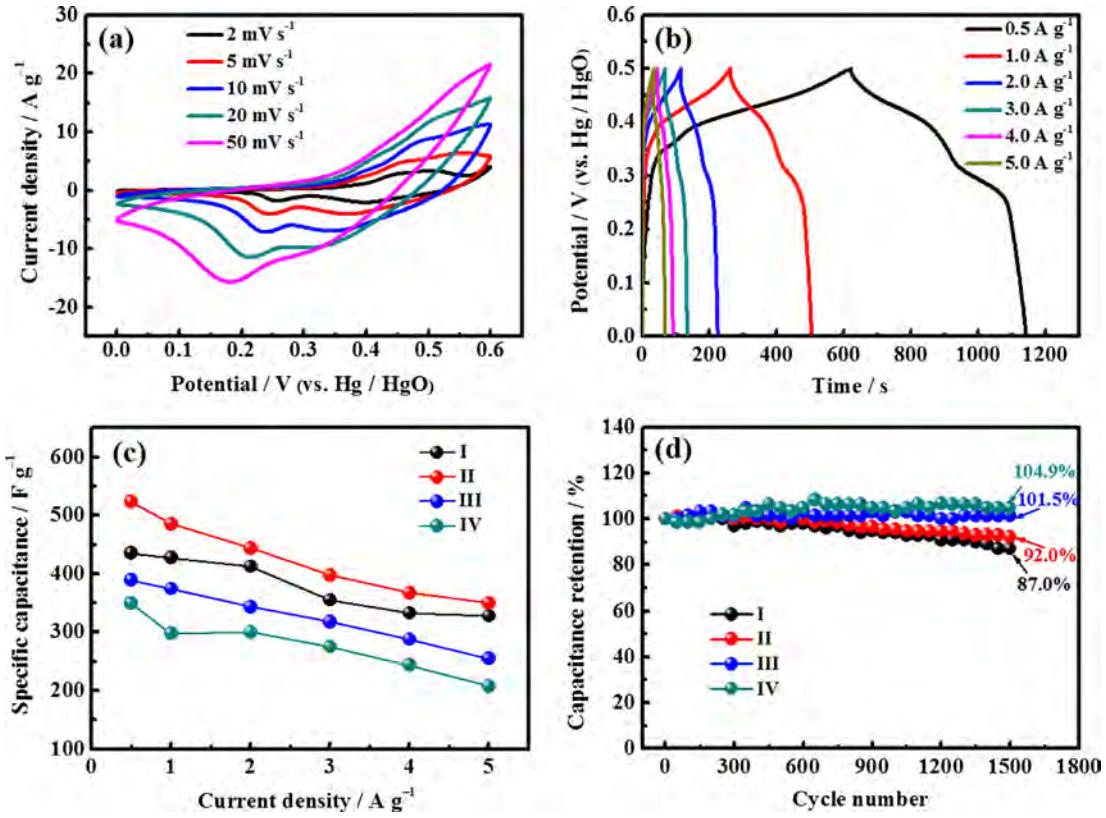

Fig. 8. (a) CV curves of the Co_3O_4 sample-II at various scan rates from 2 to 50 mV s^{-1}. (b) GCD curves of Co_3O_4 sample-II at different discharge current densities ranging from 0.5 to 5.0 A g^{-1}. (c) The corresponding specific capacitances of Co_3O_4 samples I–IV at various discharge current densities. (d) Cycling performances of Co_3O_4 samples I–IV tested for 1500 cycles at 2.0 A g^{-1}.

tion of the electrode [41]. The GCD curves of Co_3O_4 sample-II at different current densities are presented in Fig. 8b. Two discharge plateaus are noticed in all curves, which are consistent with CV behavior. The ultrafine Co_3O_4 nanoparticles exhibit specific capacitances of 523.0, 485.6, 444.0, 397.8, 367.2, and 350.0 F g^{-1} at the discharge current density of 0.5, 1.0, 2.0, 3.0, 4.0, and 5.0 A g^{-1}, respectively. The reduction of specific capacitance at higher current densities is ascribed to the electrode resistance and the decrease in efficiency utilization of the active material under higher discharge current densities [42,43]. It's noteworthy that the specific capacitance of sample-II is much higher than that of Co_3O_4 reported in other papers [10,12,40,44–48]. Interestingly, the specific capacitance of Co_3O_4 nanoparticles annealed at 250 °C is 2.6 times that of Co_3O_4 nanoflake microspheres (203.6 F g^{-1} at the current density of 0.5 A g^{-1}) which is the other product obtained in this experiment [22], probably due to the quantum size effect of the ultrafine nanoparticles. Subsequently, the rate capability of all the Co_3O_4 samples are calculated according to the GCD curves (Fig. S3) and exhibited in Fig. 8c. After a 10-fold increase in discharge current density changing from 0.5 to 5.0 A g^{-1}, 75.3%, 66.9%, 65.5%, and 59.6% of their initial specific capacitance are retained for sample-I, -II, -III, and -IV, respectively. It can be found that the rate capability of the samples correlates strongly with temperature and decreases gradually with the elevated temperature. Compared with other samples, the sample-II still exhibits good rate capability even though its rate capability is lower than that of sample-I.

Cycling performance is another key aspect for electrode materials in the practical supercapacitors. In this study, cycling performance of all as-prepared Co_3O_4 nanoparticles samples was evaluated by conducting charge–discharge tests at 2.0 A g^{-1} for 1500 cycles. As presented in Fig. 8d, after a long-term charge–discharge tests, 87.0%, 92.0%, 101.5%, and 104.9% of their initial specific capacitance can still be retained for sample-I, -II, -III, and -IV, respectively, exhibiting the excellent cycling stability of them. Apparently, the samples possessing the better cycle stability are prepared at higher temperatures. This could be attributed to that higher temperature contributes to the improvement of crystallinity and then the increment of order degree of Co_3O_4 nanoparticles in the annealing process, which makes Co_3O_4 obtained at higher temperature with higher resistance to chemical attack in the cycling charge-discharge tests. These obtained results indicate that the ultrafine Co_3O_4 nanoparticles samples have the high specific capacitance, good rate capability, and excellent cycling stability, and also suggest their high potential for practical supercapacitor applications.

4. Conclusion

In summary, we have successfully proposed a novel, facile, and eco-friendly solvothermal–precipitation method to prepare the homogeneous and ultrafine Co_3O_4 nanoparticles precursor and found the annealed products possessing superior electrochemical performance. TEM observations show that the size of the ultrafine Co_3O_4 nanoparticles is around 5–10 nm. The possible synthesis mechanism of the Co_3O_4 nanoparticles is also proposed. It is found that the annealing temperature plays an important role in the phase structure, crystallinity, crystal size, and electrochemical performances of the Co_3O_4 products. The electrochemical experiments show the samples prepared at 250 °C have the highest specific capacitance of 523.0 F g^{-1} at 0.5 A g^{-1}, which is much better than that of Co_3O_4 reported in other papers [10,12,40,44–48], mean-

while, the Co_3O_4 nanoparticles obtained at 350 °C possess the best cycling stability with capacitance retention of 104.9% after 1500 cycles, which makes them suitable for high performance supercapacitors. What's more, this study not only provides a facile approach for the fabrication of ultrafine Co_3O_4 nanoparticles with high performance but also develops an effective and widespread route for acquiring other nanomaterials in scale production.

Acknowledgements

This work was supported by the scientific and technological projects for Distinguished Young Scholars of Sichuan Province (No. 2015JQ0013); the Fundamental Research Funds for the Central Universities of China (A0920502051408; A0920502051619-72); the National Natural Science Foundation of China (No. 51602265); and China Postdoctoral Science Foundation (2016M592692).

Appendix A. Supplementary material

Supplementary data associated with this article can be found, in the online version, at http://dx.doi.org/10.1016/j.jcis.2017.06.058.

References

[1] G.P. Wang, L. Zhang, J.J. Zhang, A review of electrode materials for electrochemical supercapacitors, Chem. Soc. Rev. 41 (2012) 797–828.
[2] X.H. Lu, M.H. Yu, G.M. Wang, Y.X. Tong, Y. Li, Flexible solid-state supercapacitors: design, fabrication and applications, Energy Environ. Sci. 7 (2014) 2160–2181.
[3] V. Subramanian, H.W. Zhu, R. Vajtai, P.M. Ajayan, B.Q. Wei, Hydrothermal synthesis and pseudocapacitance properties of MnO_2 nanostructures, J. Phys. Chem. B 109 (2005) 20207–20214.
[4] C.Z. Yuan, L. Yang, L.R. Hou, L.F. Shen, X.G. Zhang, X.W. Lou, Growth of ultrathin mesoporous Co_3O_4 nanosheet arrays on Ni foam for high-performance electrochemical capacitors, Energy Environ. Sci. 5 (2012) 7883–7887.
[5] S. Park, S. Kim, Effect of carbon blacks filler addition on electrochemical behaviors of Co_3O_4/graphene nanosheets as a supercapacitor electrodes, Electrochim. Acta 89 (2013) 516–522.
[6] C.C. Xiang, M. Li, M.J. Zhi, A. Manivannan, N.Q. Wu, A reduced graphene oxide/Co_3O_4 composite for supercapacitor electrode, J. Power Sources 226 (2013) 65–70.
[7] C.Z. Yuan, B. Gao, L.F. Shen, S.D. Yang, L. Hao, X.J. Lu, F. Zhang, L.J. Zhang, X.G. Zhang, Hierarchically structured carbon-based composites: design, synthesis and their application in electrochemical capacitors, Nanoscale 3 (2011) 529–545.
[8] G.H. Yu, X. Xie, L.J. Pan, Z.N. Bao, Y. Cui, Hybrid nanostructured materials for high-performance electrochemical capacitors, Nano Energy 2 (2013) 213–234.
[9] Y.Y. Wang, Y. Lei, J. Li, L. Gu, H.Y. Yuan, D. Xiao, Synthesis of 3D-nanonet hollow structured Co_3O_4 for high capacity supercapacitor, ACS Appl. Mater. Interf. 6 (2014) 6739–6747.
[10] W. Du, R.M. Liu, Y.W. Jiang, Q.Y. Lu, Y.Z. Fan, F. Gao, Facile synthesis of hollow Co_3O_4 boxes for high capacity supercapacitor, J. Power Sources 227 (2013) 101–105.
[11] J.H. Jiang, W.D. Shi, S.Y. Song, Q.L. Hao, W.Q. Fan, X.F. Xia, X. Zhang, Q. Wang, C. B. Liu, D. Yan, Solvothermal synthesis and electrochemical performance in super-capacitors of Co_3O_4/C flower-like nanostructures, J. Power Sources 248 (2014) 1281–1289.
[12] J.C. Deng, L.T. Kang, G.L. Bai, Y. Li, P.Y. Li, X.G. Liu, Y.Z. Yang, F. Gao, W. Liang, Solution combustion synthesis of cobalt oxides (Co_3O_4 and Co_3O_4/CoO) nanoparticles as supercapacitor electrode materials, Electrochim. Acta 132 (2014) 127–135.
[13] C.Z. Yuan, L. Chen, B. Gao, L.H. Su, X.G. Zhang, Synthesis and utilization of $RuO_2{\cdot}xH_2O$ nanodots well dispersed on poly(sodium 4-styrene sulfonate) functionalized multi-walled carbon nanotubes for supercapacitors, J. Mater. Chem. 19 (2009) 246–252.
[14] W.W. Liu, X. Li, M.H. Zhu, X. He, High-performance all-solid state asymmetric supercapacitor based on Co_3O_4 nanowires and carbon aerogel, J. Power Sources 282 (2015) 179–186.
[15] Z.P. Li, X.-Y. Yu, U. Paik, Facile preparation of porous Co_3O_4 nanosheets for high-performance lithium ion batteries and oxygen evolution reaction, J. Power Sources 310 (2016) 41–46.
[16] X.X. Qing, S.Q. Liu, K.L. Huang, K.Z. Lv, Y.P. Yang, Z.G. Lu, D. Fang, X.X. Liang, Facile synthesis of Co_3O_4 nanoflowers grown on Ni foam with superior electrochemical performance, Electrochim. Acta 56 (2011) 4985–4991.
[17] L.-L. Xing, Z.-H. Chen, X.-Y. Xue, Controllable synthesis Co_3O_4 nanorods and nanobelts and their excellent lithium storage performance, Solid State Sci. 32 (2014) 88–93.
[18] L.R. Hou, C.Z. Yuan, L. Yang, L.F. Shen, F. Zhang, X.G. Zhang, Urchin-like Co_3O_4 microspherical hierarchical superstructures constructed by one-dimension nanowires toward electrochemical capacitors, RSC Adv. 1 (2011) 1521–1526.
[19] R. Tummala, R.K. Guduru, P.S. Mohanty, Nanostructured Co_3O_4 electrodes for supercapacitor applications from plasma spray technique, J. Power Sources 209 (2012) 44–51.
[20] S. Vijayakumar, A.K. Ponnalagi, S. Nagamuthu, G. Muralidharan, Microwave assisted synthesis of Co_3O_4 nanoparticles for high-performance supercapacitors, Electrochim. Acta 106 (2013) 500–505.
[21] Z.-Y. Li, P.T.M. Bui, D.-H. Kwak, M.S. Akhtar, O.-B. Yang, Enhanced electrochemical activity of low temperature solution process synthesized Co_3O_4 nanoparticles for pseudo-supercapacitors applications, Ceram. Int. 42 (2016) 1879–1885.
[22] F.Y. Liu, B.B. Zhang, H. Su, H.T. Zhang, L. Zhang, W.Q. Yang, Controllable synthesis of self-assembly Co_3O_4 nanoflake microspheres for electrochemical performance, Nanotechnology 27 (2016) 355603.
[23] M.J. Pang, G.H. Long, S. Jiang, Y. Ji, W. Han, B. Wang, X.L. Liu, Y.L. Xi, D.X. Wang, F.Z. Xu, Ethanol-assisted solvothermal synthesis of porous nanostructured cobalt oxides (CoO/Co_3O_4) for high-performance supercapacitors, Chem. Eng. J. 280 (2015) 377–384.
[24] K.S.W. Sing, D.H. Everett, L.M.R.A.W. Haul, R.A. Pierotti, J. Rouquerol, T. Siemieniewska, Reporting physisorption data for gas/solid systems with special reference to the determination of surface area and porosity, Pure Appl. Chem. 54 (1982) 2201–2218.
[25] T. He, D.R. Chen, X.L. Jiao, Y.L. Wang, Co_3O_4 nanoboxes: surfactant-templated fabrication and microstructure characterization, Adv. Mater. 18 (2006) 1078–1082.
[26] G.X. Pan, X.H. Xia, E. Cao, J. Chen, Y.J. Zhang, Template-free synthesis of hierarchical porous Co_3O_4 microspheres and their application for electrochemical energy storage, Electrochim. Acta 173 (2015) 385–392.
[27] K. Cheng, D.X. Cao, F. Yang, Y. Xu, G.H. Sun, K. Ye, J.L. Yin, G.L. Wang, Facile synthesis of morphology-controlled Co_3O_4 nanostructures through solvothermal method with enhanced catalytic activity for H_2O_2 electroreduction, J. Power Sources 253 (2014) 214–223.
[28] S.L. Wang, L.Q. Qian, H. Xu, G.L. Lü, W.J. Dong, W.H. Tang, Synthesis and structural characterization of cobalt hydroxide carbonate nanorods and nanosheets, J. Alloys Compd. 476 (2009) 739–743.
[29] D.G. Klissurski, E.L. Uzunova, Synthesis of nickel cobaltite spinel from coprecipitated nickel-cobalt hydroxide carbonate, Chem. Mater. 3 (1991) 1060–1063.
[30] J.J. Yang, H. Cheng, R.L. Frost, Synthesis and characterisation of cobalt hydroxy carbonate $Co_2CO_3(OH)_2$ nanomaterials, Spectrochim. Acta Part A 78 (2011) 420–428.
[31] M. Nassar, I. Ahmed, Template-free hydrothermal derived cobalt oxide nanopowders: synthesis, characterization, and removal of organic dyes, Mater. Res. Bull. 47 (2012) 2638–2645.
[32] D.H. Wang, S.E. Hui, C.C. Liu, H.Y. Zhuang, Effect of oxygen and additives on thermal decomposition of aqueous urea solution, Fuel 180 (2016) 34–40.
[33] P.M. Schaber, J. Colson, S. Higgins, D. Thielen, B. Anspach, J. Brauer, Thermal decomposition (pyrolysis) of urea in an open reaction vessel, Thermochim. Acta 424 (2004) 131–142.
[34] B.X. Li, Y. Xie, C.Z. Wu, Z.Q. Li, J. Zhang, Selective synthesis of cobalt hydroxide carbonate 3D architectures and their thermal conversion to cobalt spinel 3D superstructures, Mater. Chem. Phys. 99 (2006) 479–486.
[35] M.Y. Nassar, I.S. Ahmed, Hydrothermal synthesis of cobalt carbonates using different counter ions: an efficient precursor to nano-sized cobalt oxide Co_3O_4, Polyhedron 30 (2011) 2431–2437.
[36] B. Choi, G. Kim, K. Yi, J. Kim, W. Hong, Influence of operating temperature on CO_2-NH_3 reaction in an aqueous solution, Korean J. Chem. Eng. 29 (2011) 478–482.
[37] S.Y. Park, K.B. Yi, C.H. Ko, J.-H. Park, J.-N. Kim, W.H. Hong, Selection of optimal operating conditions for a continuous CO_2-capture process using an aqueous ammonia solution, Energy Fuels 24 (2010) 3704–3709.
[38] X.H. Xia, J.P. Tu, Y.J. Mai, X.L. Wang, C.D. Gu, X.B. Zhao, Self-supported hydrothermal synthesized hollow Co_3O_4 nanowire arrays with high supercapacitor capacitance, J. Mater. Chem. 21 (2011) 9319–9325.
[39] B.R. Duan, Q. Cao, Hierarchically porous Co_3O_4 film prepared by hydrothermal synthesis method based on colloidal crystal template for supercapacitor application, Electrochim. Acta 64 (2012) 154–161.
[40] Y.Q. Zhang, L. Li, S.J. Shi, Q.Q. Xiong, X.Y. Zhao, X.L. Wang, C.D. Gu, J.P. Tu, Synthesis of porous Co_3O_4 nanoflake array and its temperature behavior as pseudo-capacitor electrode, J. Power Sources 256 (2014) 200–205.
[41] W.L. Yang, Z. Gao, J. Ma, J. Wang, B. Wang, L.H. Liu, Effects of solvent on the morphology of nanostructured Co_3O_4 and its application for high-performance supercapacitors, Electrochim. Acta 112 (2013) 378–385.
[42] T. OuYang, K. Cheng, S.Y. Kong, K. Ye, Y.Y. Gao, D.F. Zhang, G.L. Wang, D.X. Cao, Facile synthesis of Co_3O_4 with different morphology and their application in supercapacitors, RSC Adv. 5 (2015) 36059–36065.
[43] M. Huang, Y.X. Zhang, F. Li, L.L. Zhang, Z.Y. Wen, Q. Liu, Facile synthesis of hierarchical Co_3O_4@MnO_2 core–shell arrays on Ni foam for asymmetric supercapacitors, J. Power Sources 252 (2014) 98–106.
[44] R.-T. Wang, L.-B. Kong, J.-W. Lang, X.-W. Wang, S.-Q. Fan, Y.-C. Luo, L. Kang, Mesoporous Co_3O_4 materials obtained from cobalt–citrate complex and their high capacitance behavior, J. Power Sources 217 (2012) 358–363.

[45] H. Pang, F. Gao, Q. Chen, R.M. Liu, Q.Y. Lu, Dendrite-like Co_3O_4 nanostructure and its applications in sensors, supercapacitors and catalysis, Dalton Trans. 41 (2012) 5862–5868.
[46] F. Meng, Z. Fang, Z. Li, W. Xu, M. Wang, Y. Liu, J. Zhang, W. Wang, D. Zhao, X. Guo, Porous Co_3O_4 materials prepared by solid-state thermolysis of a novel Co-MOF crystal and their superior energy storage performances for supercapacitors, J. Mater. Chem. A 1 (2013) 7235–7241.
[47] H. Du, L. Jiao, Q. Wang, J. Yang, L. Guo, Y. Si, Y. Wang, H. Yuan, Facile carbonaceous microsphere templated synthesis of Co_3O_4 hollow spheres and their electrochemical performance in supercapacitors, Nano Res. 6 (2012) 87–98.
[48] K.B. Wang, X. Yi, X. Luo, Y. Shi, J. Xu, Fabrication of Co_3O_4 pseudocapacitor electrodes from nanoscale cobalt–organic frameworks, Polyhedron 109 (2016) 26–32.